ANOMALOUS TRANSPORT AND UNSTABLE MODES IN NEUTRAL-BEAM-HEATED L AND H PLASMAS OF ASDEX

G. Becker

IPP III/100 January 1985

MAX-PLANCK-INSTITUT FÜR PLASMAPHYSIK

8046 GARCHING BEI MÜNCHEN

MAX-PLANCK-INSTITUT FÜR PLASMAPHYSIK

GARCHING BEI MÜNCHEN

ANOMALOUS TRANSPORT AND UNSTABLE MODES IN NEUTRAL-BEAM-HEATED L AND H PLASMAS OF ASDEX

G. Becker

IPP III/100 January 1985

Die nachstehende Arbeit wurde im Rahmen des Vertrages zwischen dem Max-Planck-Institut für Plasmaphysik und der Europäischen Atomgemeinschaft über die Zusammenarbeit auf dem Gebiete der Plasmaphysik durchgeführt.

IPP III/100 G. Becker

ANOMALOUS TRANSPORT AND UNSTABLE MODES IN NEUTRAL-BEAM-HEATED L AND H PLASMAS OF ASDEX

(January 1985)

ABSTRACT. It is attempted to determine the type of instabilities responsible for anomalous transport in the L and H regimes. Resistive and ideal ballooning as well as pressure-driven modes are found to be stable. There is seen no clear correlation between the electron heat diffusivity in L discharges and the extent of the banana zone. With $\nu_{*e} < 1$ and $\nu_{*i} < 1$ dissipative trapped-electron and trapped-ion modes should be the dominant drift instabilities in L and H discharges. The time evolution of $\eta_{e,i} = d\ln T_{e,i}/d\ln n$ is shown to be correlated with L and H transport. The operational limits of the H regime are found to be connected with variations of $\eta_{e,i}$, which primarily result from changing the heating profile of injection and the beam fuelling.

1. Introduction

Axisymmetric divertor tokamaks have proved to be capable of producing clean plasmas with ohmic heating and even with strong neutral-injection heating. A further benefit of divertor tokamaks is that with beam heating a high-confinement type of operation denoted as the H mode /1,2,3/ is accessible under certain operating conditions.

Results from earlier transport simulations of neutral-beam-heated L (low-confinement) and H discharges in ASDEX have been reported in Refs. /4-6/. In this report the L and H confinement is investigated with respect to the underlying unstable modes. This is done in Section 2.1 by selecting the instabilities which can cause the observed anomalous energy and particle fluxes with neutral injection and by looking for correlations of the confinement properties with the time evolution of the collisionality factors ν_{*e} and ν_{*i}. Then, in Section 2.2, the peculiarities of transport in the L and H regimes are compared with specific linear stability features of trapped-particle instabilities. Finally, in Section 3, the conclusions of these studies are summarized.

2. Instabilities and local transport in L and H plasmas

Usually, the anomalous transport observed in tokamaks is ascribed to turbulent field fluctuations excited by instabilities. The fluctuation level of microturbulence, the wave-number spectra and the scalings of diffusivities depend on the saturation processes in non-linear growth of the instabilities. As theory fails at present to solve these formidable problems, reliable microinstability-based anomalous diffusivities are not available. It is therefore attempted to find correlations between known local transport properties in neutral-beam-heated plasmas and specific linear stability features.

Linear stability theory is important for confinement studies insofar as it can serve to select the unstable modes which cause the anomalous particle and heat fluxes. The most important instabilities that have to be considered for ASDEX plasmas are resistive and ideal ballooning modes, pressure-driven modes and drift modes.

2.1 Stable and unstable modes in L and H discharges

Owing to the high electron temperatures and correspondingly large electrical conductivity in L and H plasmas of ASDEX the linear growth rates of resistive ballooning modes are only very small. Highly unstable plasmas are anticipated for $S(r=0) = \tau_{res}/\tau_A \approx 10^5$ to 10^6, where τ_{res} and τ_A are the resistive and Alfvén times, respectively, while in the L and H phases typical S values are 10^8. According to Ref. /7/ the saturation level strongly decreases as S increases. Resistive pressure-driven modes in ASDEX are thus only weakly unstable and should produce very low fluctuation levels. Moreover, recent theoretical work has shown that resistive ballooning modes may be completely stabilized if finite parallel electron heat conductivity /8/ or parallel viscosity are taken into account.

A criterion for stability of ideal ballooning modes which can also serve as a first-order estimate of the ideal MHD stability limit of pressure-driven modes is given by /9/

$$-\frac{2 R_o q^2}{B_t^2}\frac{\partial p}{\partial r} \leq f(s), \qquad (1)$$

where $q = rB_t/(R_o B_p)$ and $f(s)$ is a function of the dimensionless shear $s = (r/q)\frac{\partial q}{\partial r}$. According to this criterion the analyzed L and H plasmas are

stable against ideal ballooning and pressure-driven modes. This conclusion is supported by the result that for B_t = 2.2 T the volume-averaged $ß_t$ values including the beam contribution are only about 1 %. Stability analysis with the ERATO code /10/ has shown that the free-boundary equilibria based on measured profiles are stable against ideal ballooning and kink modes.

It is obvious that these instabilities cannot cause the enhanced losses, which even occur in L discharges with low poloidal beta ($ß_p$ = 0.3) and rather small injection power P_{NI} of about the ohmic input /5/. Raising P_{NI} and $ß_p$ results in a smooth increase of the electron heat diffusivity. A change in scaling due to the possible onset of pressure-driven modes is not seen. We conclude that the anomalous particle and heat fluxes in L and H plasmas do not result from ideal ballooning and pressure-driven instabilities.

In order to select possible candidates from the large family of drift instabilities, the radial extent and time development of collisionality regimes in OH, L and H discharges are determined. It is found that in the ohmic phases prior to and after neutral injection electrons and ions reach the banana regime ($\nu_{*e} < 1$, $\nu_{*i} < 1$) typically in the range 11 < r < 25 cm as shown in Fig. 1 with $\bar{n} = 4.2 \times 10^{13}$ cm^{-3}. For the collisionality factors of Fig. 1 theory predicts universal drift instabilities (plateau regime) and trapped-particle instabilities (banana regime). Neutral injection enlarges the banana zone over most of the plasma within the separatrix (see Fig. 2). A typical range in L and H plasmas is 4 < r < 39 cm. Both electrons and ions are highly collisionless. In some cases ν_{*i} values as small as 10^{-2} have been reached locally. In the L and H plasmas the prevailing drift modes are the trapped-particle instabilities. Collisionless trapped-particle modes can be excluded, since the condition

$$\frac{\lambda_e \varrho_i}{r^2} \gg \left(\frac{m_i}{m_e}\right)^{1/2}, \qquad (2)$$

where λ_e is the electron mean-free path and ϱ_i is the ion gyroradius, is not satisfied /11/. Both dissipative trapped-electron instabilities ($\nu_{*e} < 1$) and dissipative trapped-ion instabilities (ν_{*e}, $\nu_{*i} < 1$) have to be taken into account and are possibly responsible for the L and H transport.

Simulations of L discharges have shown that after the beams are switched on the confinement of ohmic discharges continues for some time $(\Delta t)_{on}$ before the enhanced transport occurs /4,5/. There is also found a time difference

$(\Delta t)_{off}$ between the end of the degraded confinement and the end of the beam heating. This time evolution exhibits some parallels with that of the expansion of the banana region over the confinement zone ($r_{q=1} < r < r_s$ with separatrix radius r_s). Nevertheless, a clear correlation with the collisionality parameters ν_{*e} and ν_{*i} cannot be demonstrated. One problem, particularly at small densities, is that a large banana zone can already exist during the ohmic phases which does not seem to change the OH confinement (e.g. $\nu_{*e} < 1$ in the zone $10 < r < 31$ cm at $\bar{n}_e = 2.5 \times 10^{13}$ cm^{-3}).

A very characteristic time development of H discharges is observed. They are found to pass through the phases OH-L-H-L-OH, i.e. the H phase always develops from an L discharge and returns to an L phase. This indicates that the same instabilities are responsible for the L and H confinement. Such a conclusion is also supported by the parallels in empirical scaling of the electron thermal diffusivity, i.e. $\chi_e \sim T_i^{1/2} B_p^{-1}$ in the L and H regimes /5,12/.

The mode frequency of trapped-electron instabilities has to satisfy the inequality

$$\omega_{bi}, \omega_{ti} < \omega < \omega_{be}, \omega_{te}, \tag{3}$$

where

$$\omega_{be,i} = \left(\frac{r}{R_o}\right)^{1/2} v_{e,i} (q R_o)^{-1} \tag{4}$$

are the electron and ion bounce frequencies and

$$\omega_{te,i} = k_{\parallel} v_{e,i} \tag{5}$$

are the electron and ion transit frequencies. The mode frequencies ω are close to the electron diamagnetic drift frequency

$$\omega_{*e} = \frac{c T_e m}{e B r r_n}, \tag{6}$$

where m is the poloidal mode number and $r_n = -n/\frac{\partial n}{\partial r}$ is the density scale length. In L and H plasmas dissipative trapped-electron modes can be unstable for $m \gtrsim 15$, where $\omega > \omega_{bi}$ is satisfied. An important parameter is

$$\eta_e = \frac{d\ln T_e}{d\ln n} = \frac{r_n}{r_{Te}} \tag{7}$$

with the electron temperature scale length $r_{Te} = -T_e/\frac{\partial T_e}{\partial r}$.

For poloidal wave numbers $m \lesssim 15$ it holds that

$$\omega < \omega_{bi}, \omega_{ti} \tag{8}$$

so that dissipative trapped-ion instabilities can be generated. An important parameter for these modes /13/ is

$$\eta_i = \frac{d\ln T_i}{d\ln n} = \frac{r_n}{r_{Ti}} \tag{9}$$

with the ion temperature scale length $r_{Ti} = -T_i/\frac{\partial T_i}{\partial r}$. The parameters η_e and η_i are evaluated from measured density and temperature profiles. Where complete experimental profiles are not available, results from simulations which fit these profiles and the measured energy confinement times and β_p values are used. In the special case of similar density and temperature profiles η_e, $\eta_i \approx 1$ result which are radially constant even if r_n and $r_{Te,i}$ exhibit a strong r dependence. The η_i values in L and H plasmas are found to exceed 2/3, which is critical for ion Landau damping. For $\eta_i > 2/3$ the contributions due to untrapped ions at the transit resonance and due to trapped ions at the bounce resonance become destabilizing /14/. According to Ref. /13/ the other critical η_i value is 1.75. Below this limit ion collisional damping is favourable, whereas it is destabilizing above.

A stability diagram for the dissipative trapped-ion mode /13/ in an H discharge with $\eta_e(2r_s/3) = 1.1$ and $\eta_i(2r_s/3) = 1.4$ is shown in Fig. 3. The quantities a and l are the plasma radius and toroidal mode number ($lq \simeq m$), respectively. The lines labelled $\gamma_e = \omega_o$ and $\omega_o = \omega_{bi}$ represent conditions for the existence of dissipative trapped-ion modes /13/, where ω_o is the mode frequency. Obviously, the smallest l and m values are stable in H discharges owing to ion collisional damping.

More sophisticated models of the dissipative trapped-ion instability which include effects such as shear /15/ and magnetic (∇B) drifts /16,17/ lead to less restrictive stability requirements. It is expected that η_i qualitatively plays the same role as before, although in realistic situations critical η_i values for local stability should no longer exist.

The very specific features of the L and H confinement make it promising to

look for correlations with trapped-particle instabilities.

2.2 Connection between η values and operational limits

As the time evolutions of η_e and η_i are rather similar, it is sufficient to look for parallels between η_i and local transport. The η_i values and scale lengths r_n and r_{Ti} presented are evaluated near the middle of the confinement zone at $r = 2r_s/3$. Comparing a large number of L and H discharges shows that the η values are smaller in the H regime. The time behaviour of $\eta_i(2r_s/3)$ is quite different in L discharges with $\bar{n}$ well below the critical density $\bar{n}_{cr}$ for reaching the H regime and in H discharges with $\bar{n}$ well above that limit, as shown in Fig. 4. Obviously, in the L discharge the η_i values continue to be large. In H discharges, the time development of η_i corresponds to the observed sequence of phases OH-L-H-L-OH. After the beams are turned on, η_i decreases monotonically, while the plasma passes through the L phase and, for sufficiently small values, reaches the H phase. After the beams are turned off and the fast ions have slowed down, fuelling and heating by neutral injection are negligibly small. The resulting peaking of temperature profiles due to ohmic heating leads to a rapid increase of η_i, which soon terminates the H confinement, and the phases are run through in the opposite direction. For values of the injection power below 3.2 MW the parameters η_e and η_i decrease more slowly than shown in Fig. 4, so that the transition to the H phase should occur later. This agrees with the experimental observation that reducing the injection power leads to later L-to-H transitions.

The variation of η_i, r_n and r_{Ti} with $\bar{n}$ is shown in Fig. 5 (I_p = 380 kA, P_{NI} = 2.5 MW). As can be seen, smaller η_i values are obtained in the H regime with densities above the critical value $\bar{n}_{cr} \simeq 3.4 \times 10^{13}$ cm^{-3}. The weak increase of r_n with larger $\bar{n}$ results from the fact that the dominant particle source, i.e. ionization of cold neutrals near the separatrix, is somewhat shifted to the edge. The ion temperature scale length r_{Ti}, however, exhibits a faster rise owing to the strong broadening of beam-heating profiles with larger target densities. That the variation of η_e and η_i with $\bar{n}$ indeed mainly results from changing the profile of the beam power density is illustrated in Fig. 6. Obviously, there is a very steep dependence of the heating profile on $\bar{n}$. Over the full range of density variation $\bar{n}$ = 1.5 to 8 x 10^{13} cm^{-3} the change in profile is even larger.

At low densities ($\bar{n} \simeq 2.4 \times 10^{13}$ cm^{-3}) short $r_{Ti}(2r_s/3)$ of about 14 cm are

found for both ohmically heated and beam-heated discharges with various injection powers. Beam heating here is as peaked as the ohmic heating profile so that large $\eta_{e,i}$ values result and the plasma stays in the L regime for all injection powers.

The situation is quite different for $\bar{n} = 4.5 \times 10^{13}$ cm^{-3}, as shown in Fig. 7. Here, r_{Ti} increases owing to the broader beam-heating profile if the injection power exceeds the ohmic input. While fuelling due to cold neutrals takes place close to the separatrix, neutral injection represents a particle source for the bulk plasma. This explains the decrease of r_n with increasing beam fuelling. The L and H regimes again correspond to large and small η values, respectively. The regimes are separated by the critical injection power, which amounts to 1.9 MW for the double-null configuration.

Moreover, the model is consistent with the observation that limiter discharges and divertor discharges with strong influx of neutral hydrogen or light impurities in the main chamber are in the L regime. The energy losses in the outer plasma cause peaked temperature profiles and large η values.

As the more sophisticated linear stability theory of dissipative trapped-particle modes does not predict sharp η_e or η_i limits, the rather abrupt L-to-H transition cannot be explained by the correlation of η values with L and H transport only. Indeed, there are experimental indications that this transition is triggered by rapid profile changes due to processes near the separatrix.

3. Conclusions

The stability of modes which are thought to be most important for injection-heated ASDEX plasmas has been studied. It is found that resistive ballooning, ideal ballooning and pressure-driven instabilities are stable and thus cannot contribute to the observed anomalous losses. Both dissipative trapped-electron and trapped-ion modes are unstable in the L and H plasmas and should be the prevailing drift instabilities.

Owing to neutral-beam heating electrons and ions in the confinement zone ($r_{q=1} < r < r_s$) reach the banana regime defined by $\nu_{*e} < 1$ and $\nu_{*i} < 1$. The delay times $(\Delta t)_{on}$ and $(\Delta t)_{off}$ for the enhanced losses in L discharges cannot be correlated with the time evolution of the collisionality

parameters. The large differences in empirical scaling of local transport between ohmically heated ($\chi_e^{OH} \sim n_e^{-1} T_e^{-1} q^{-1}$) and injection-heated plasmas ($\chi_e^{L,H} \sim T_i^{1/2} B_p^{-1}$) appear to be due to the transition to a different type of instability which mainly excites turbulence in the confinement zone. Trapped-particle instabilities are found to be likely candidates.

The time evolution of the profile parameters $\eta_{e,i} = r_n/r_{Te,i}$ is found to be correlated with L and H transport and with the sequence of phases OH-L-H-L-OH passed through in H discharges. The L and H regimes correspond to large and small $\eta_{e,i}$ values, respectively. For $\bar{n} > \bar{n}_{cr}$ small η values result, so that the H regime is accessible, whereas at low densities peaked temperature profiles corresponding to large η are obtained (L regime). The operational limits for reaching the H mode, i.e. the minimum line-averaged density and the minimum injection power, can be qualitatively explained in terms of the parameters $\eta_{e,i}$. Limiter discharges and divertor discharges with strong influx of neutral hydrogen or light impurities exhibit more peaked temperature profiles. According to the model they persist in the L regime owing to large η values.

The variation of η_e and η_i with the plasma parameters is found to be primarily due to changing the heating profiles of neutral injection. This becomes obvious from the very sensitive dependence of the absorbed beam power profile on the target density in the range of $\bar{n}$ variation.

According to this trapped-particle model the H regime should be accessible for heating systems which yield sufficiently broad temperature profiles. Ohmic-heating as well as beam-heating profiles at small target densities are peaked too much, while at higher densities sufficiently broad profiles are obtained with neutral injection. These studies underline the importance of heating profiles for confinement.

Acknowledgement

Valuable discussions with Dr. D. Biskamp are appreciated.

References

/1/ Wagner, F., Becker, G., Behringer, K., Campbell, D., Eberhagen, A., et al., Phys. Rev. Lett. 49 (1982) 1408.

/2/ Wagner, F., Becker, G., Behringer, K., Campbell, D., Eberhagen, A., et al., Plasma Physics and Controlled Nuclear Fusion Research 1982 (Proc. 9th Int. Conf. Baltimore, 1982) Vol. 1, IAEA, Vienna (1983) 43.

/3/ Keilhacker, M., Becker, G., Bernhardi, K., Eberhagen, A., ElShaer, M., et al., Plasma Physics and Contr. Fusion 26 (1984) 49.

/4/ Becker, G., ASDEX Team, Neutral Injection Team, Nuclear Fusion 22 (1982) 1589.

/5/ Becker, G., Campbell, D., Eberhagen, A., Gehre, O., Gernhardt, J., et al., Nuclear Fusion 23 (1983) 1293.

/6/ Becker, G., et al., Proc. 11th Europ. Conf. on Contr. Fusion and Plasma Physics, Aachen 1983, Vol. II, p. 299.

/7/ Carreras, B.A., Diamond, P.H., Murakami, M., Dunlap, J.L., Bell, J.D., et al., Phys. Rev. Lett. 50 (1983) 503.

/8/ Sundaram, A.K., Sen, A., and Kaw, P.K., Phys. Rev. Lett. 52 (1984) 1617.

/9/ Connor, J.W., Hastie, R.J. and Taylor, J.B., Phys. Rev. Lett. 40 (1978) 396.

/10/ Kerner, W., private communication.

/11/ Kadomtsev, B.B., Pogutse, O.P., Nuclear Fusion 11 (1971) 67.

/12/ Becker, G., ASDEX Team and Neutral Injection Team Report IPP III/98; Becker, G., Nuclear Fusion 24 (1984) 1364.

/13/ Rosenbluth, M.N., Ross, D.W., Kostomarov, D.P., Nuclear Fusion 12 (1972) 3.

/14/ Tang, W.M., Nuclear Fusion 18 (1978) 1089.

/15/ Gladd, N.T., Ross, D.W., Phys. Fluids 16 (1973) 1706.

/16/ Tang, W.M., Phys. Fluids 17 (1974) 1249.

/17/ Tagger, M., Laval, G., Pellat, R., Nuclear Fusion 17 (1977) 109.

Figure Captions

Fig. 1: Radial extent of banana and plateau regimes in the ohmic phase ($\bar{n} = 4.2 \times 10^{13}$ cm^{-3}).

Fig. 2: Typical extent of banana zone in L and H discharges.

Fig. 3: Stability diagram for dissipative trapped-ion modes in an H discharge of ASDEX with $\eta_e(2r_s/3) = 1.1$ and $\eta_i(2r_s/3) = 1.4$. The points with different toroidal wave numbers 1 lie on a line of slope 3/2.

Fig. 4: Time behaviour of η_i in an L discharge with $\bar{n} = 2.5 \times 10^{13}$ cm^{-3} ($I_p = 380$ kA, $P_{NI} = 2.5$ MW) and in an H discharge with $\bar{n} = 4.2 \times 10^{13}$ cm^{-3} ($I_p = 380$ kA, $P_{NI} = 3.2$ MW).

Fig. 5: η_i and scale lengths r_n and r_{Ti} vs. $\bar{n}$ for $I_p = 380$ kA and $P_{NI} = 2.5$ MW.

Fig. 6: Profiles of power density S_b due to neutral-beam heating at two target densities.

Fig. 7: η_i and scale lengths r_n and r_{Ti} vs. P_{NI} for $I_p = 380$ kA and $\bar{n} = 4.5 \times 10^{13}$ cm^{-3}.

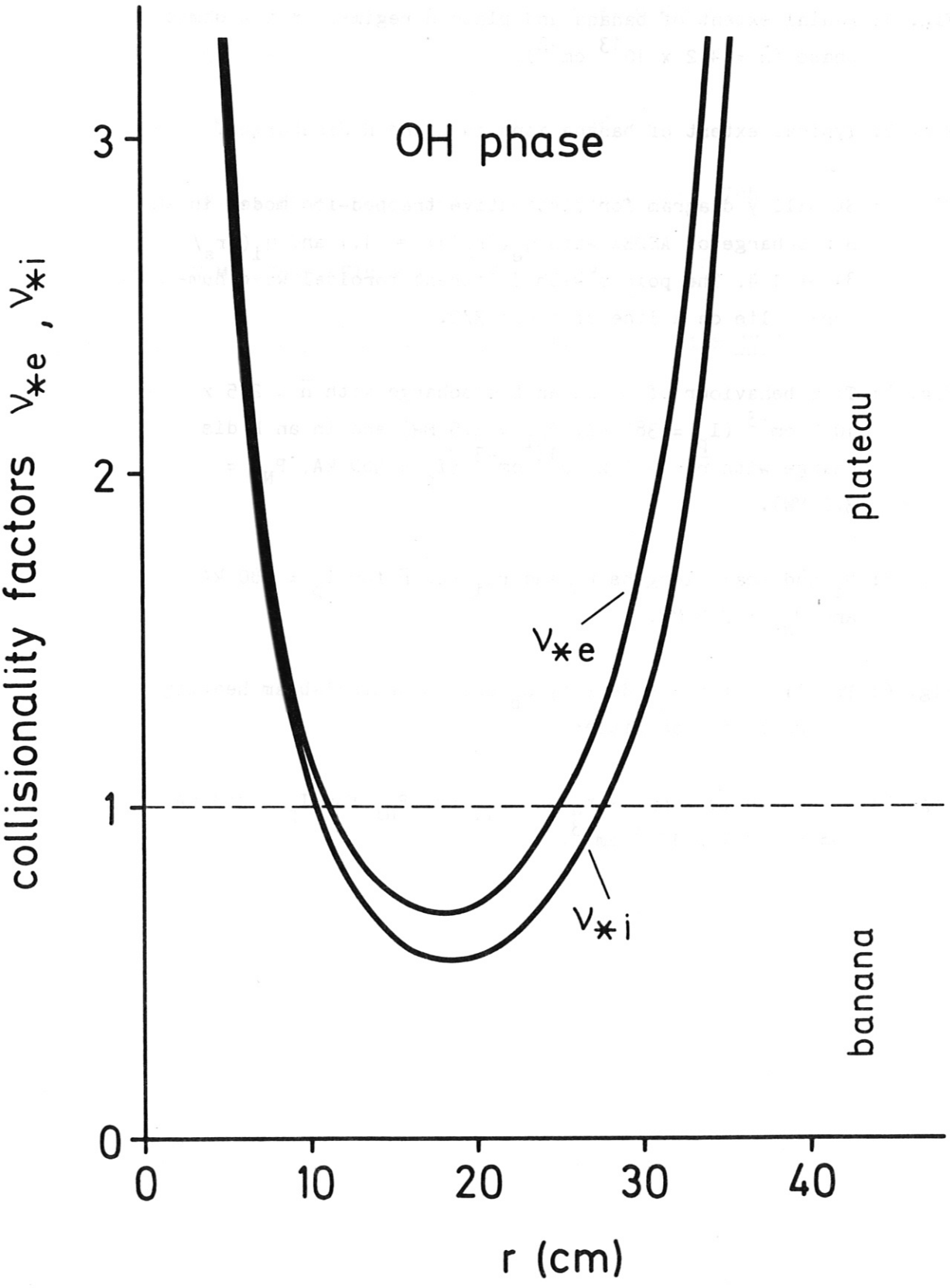
OH phase
collisionality factors ν_{*e} , ν_{*i}
3
2
1
0
0
10
20
30
40
r (cm)
ν_{*e}
ν_{*i}
plateau
banana
IPP3- BEC 047-84

Fig. 1

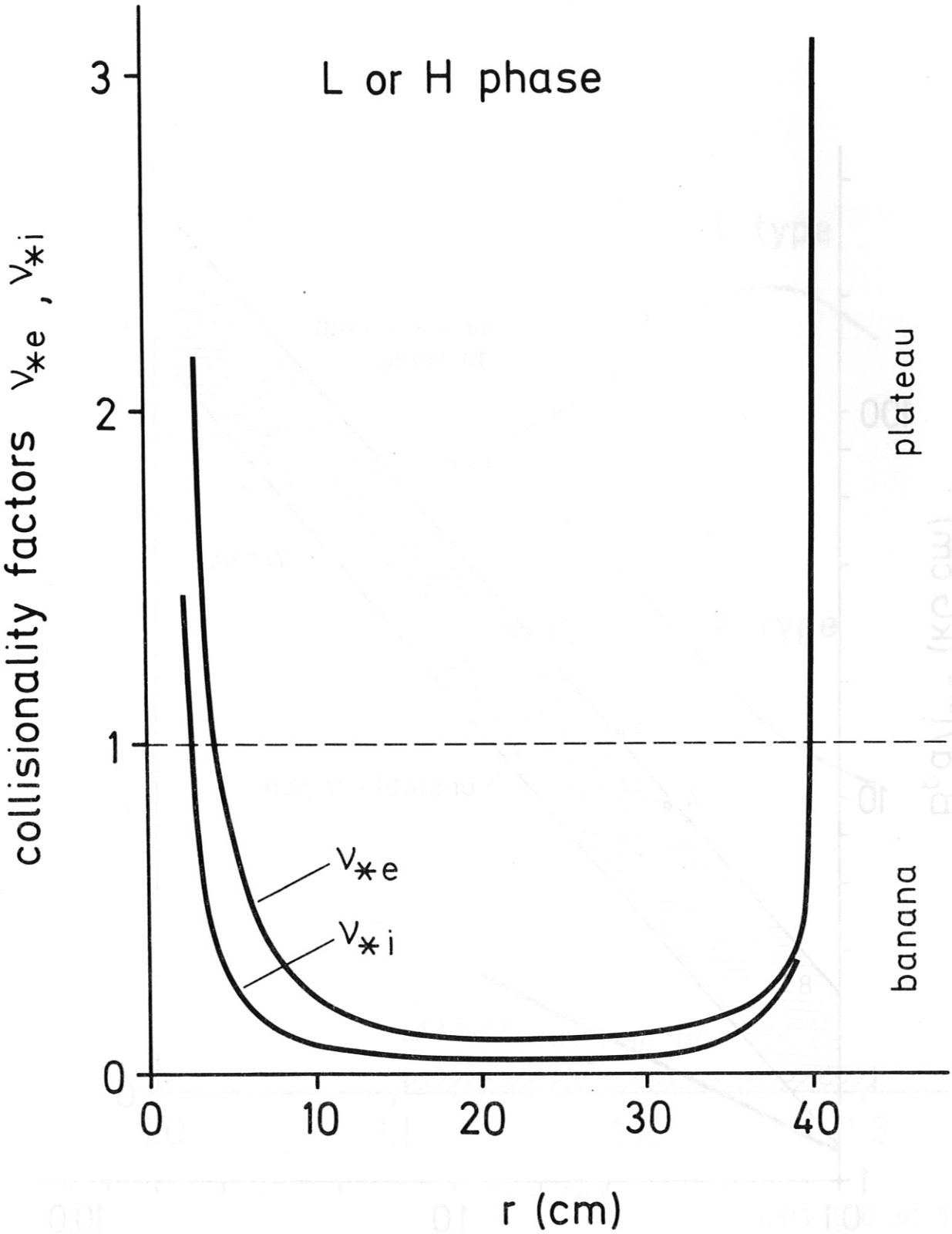
L or H phase
collisionality factors ν_{*e} , ν_{*i}
3
2
1
0
0
10
20
30
40
r (cm)
ν_{*e}
ν_{*i}
plateau
banana
IPP3-BEC 189-84

Fig. 2

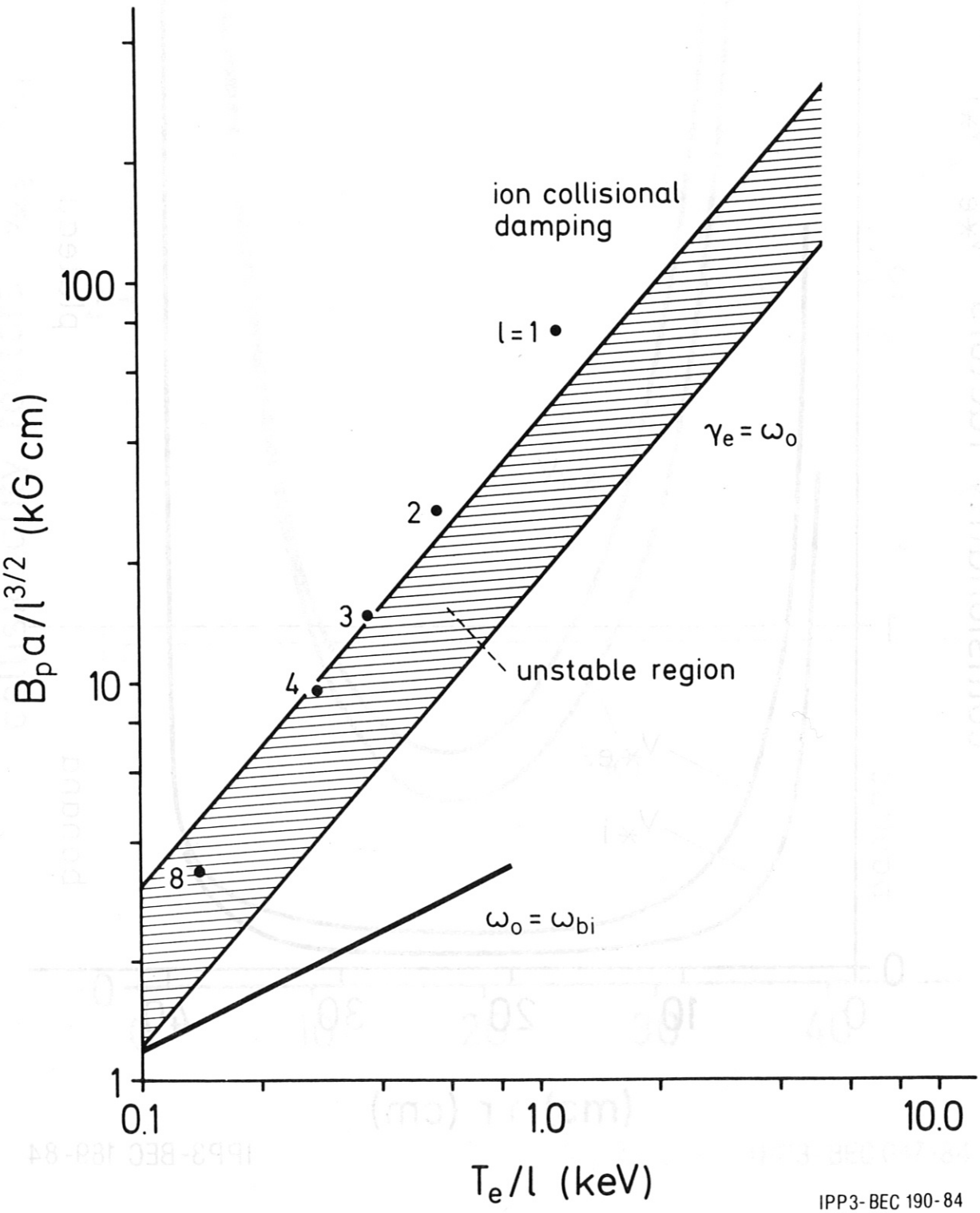
ion collisional
damping
l = 1
2
3
4
8
$\gamma_e = \omega_o$
unstable region
$\omega_o = \omega_{bi}$
100
10
1
0.1
1.0
10.0
$B_p a / l^{3/2}$ (kG cm)
T_e / l (keV)
IPP3-BEC 190-84

Fig. 3

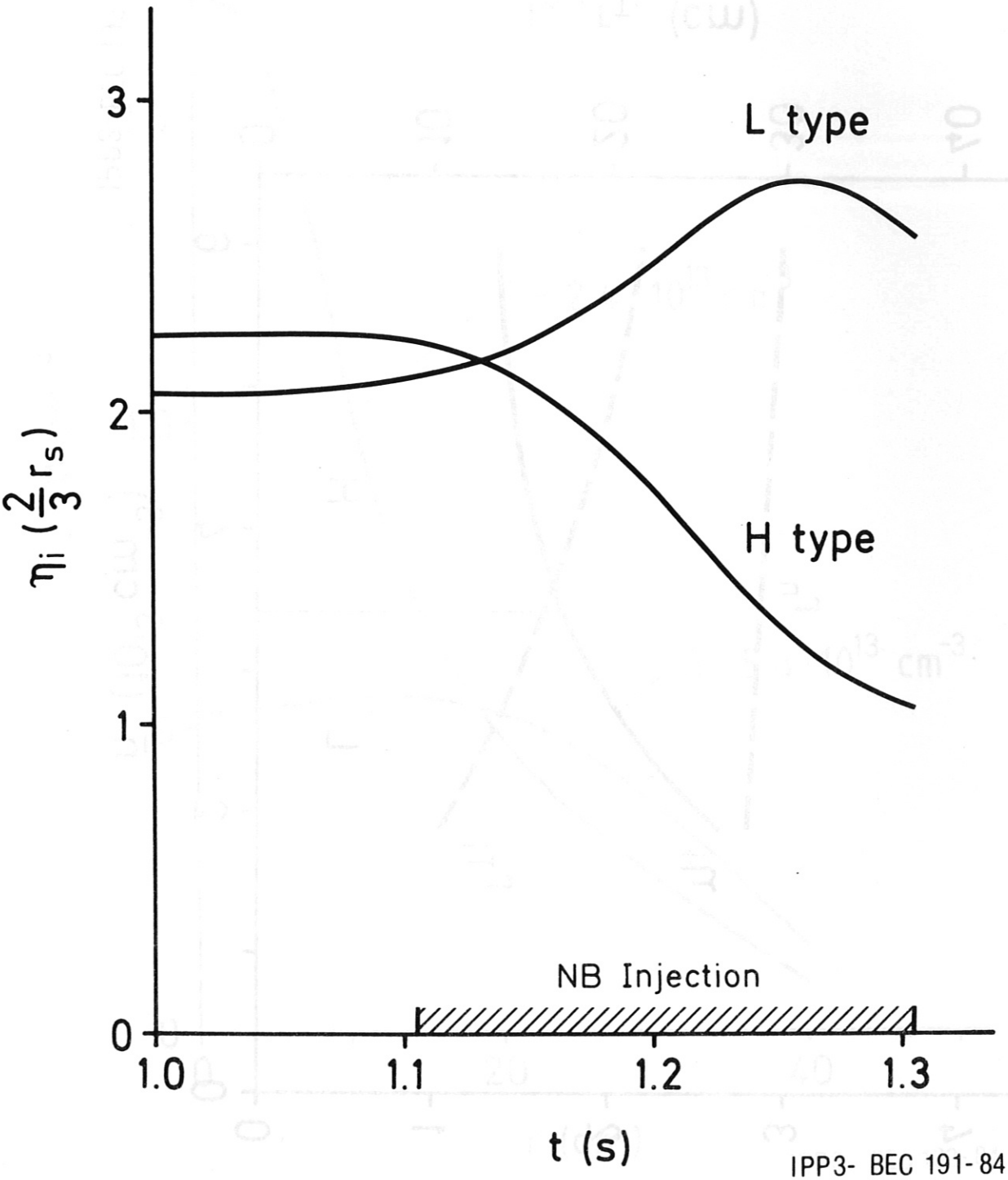
3
2
1
0
L type
H type
$\eta_i\,(\frac{2}{3}r_s)$
NB Injection
1.0
1.1
1.2
1.3
t (s)
IPP3- BEC 191-84

Fig. 4

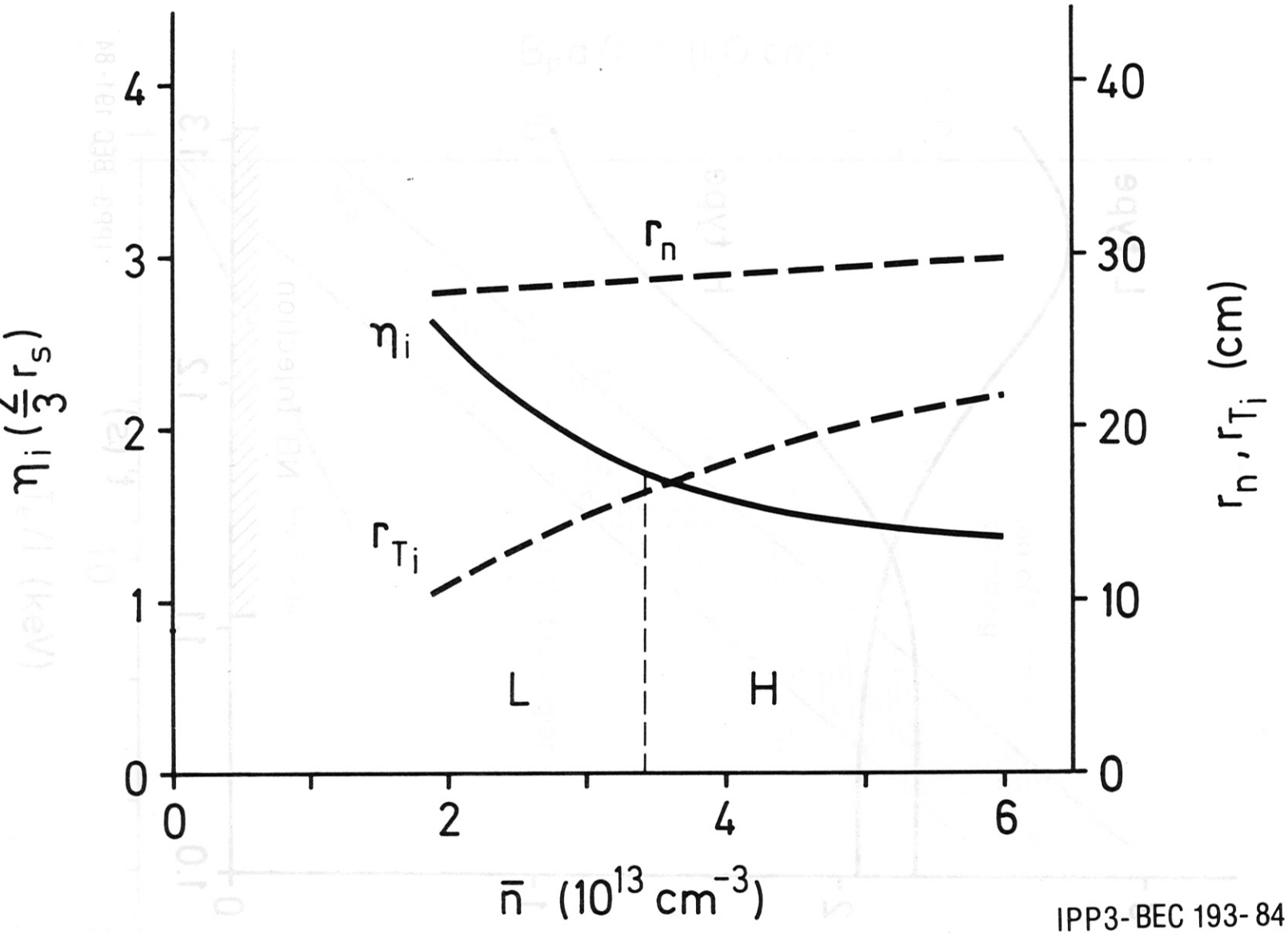
$\eta_i(\frac{2}{3}r_s)$
r_n, r_{Ti} (cm)
r_n
η_i
r_{Ti}
L
H
$\bar{n}$ (10^{13} cm^{-3})
0
1
2
3
4
0
10
20
30
40
0
2
4
6
IPP3-BEC 193-84

Fig. 5

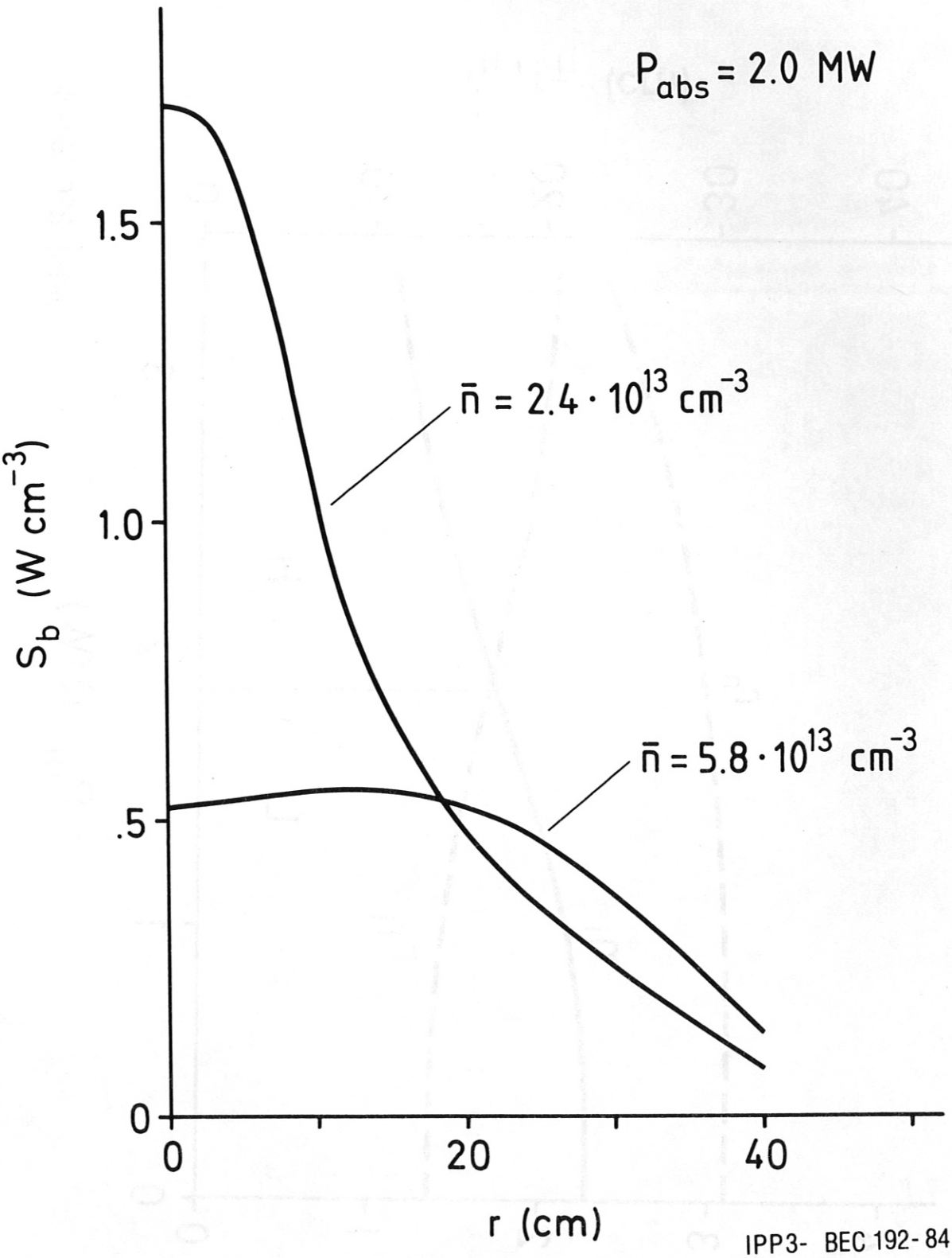
P_{abs} = 2.0 MW
$\bar{n} = 2.4 \cdot 10^{13}$ cm^{-3}
$\bar{n} = 5.8 \cdot 10^{13}$ cm^{-3}
S_b (W cm^{-3})
1.5
1.0
.5
0
0
20
40
r (cm)
IPP3- BEC 192-84

Fig. 6

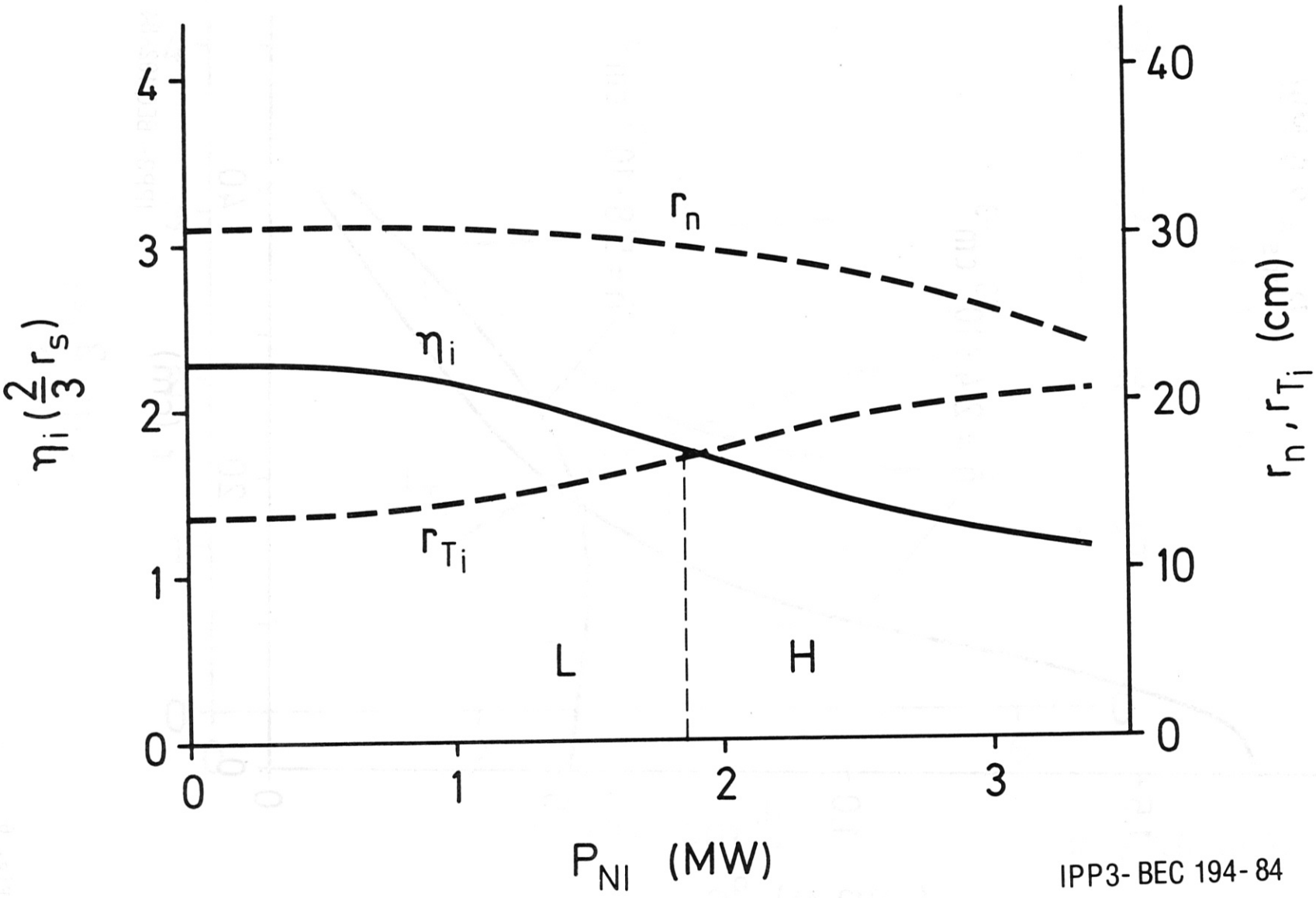
$\eta_i(\frac{2}{3}r_s)$
4
3
2
1
0
0
1
2
3
P_{NI} (MW)
r_n
η_i
r_{Ti}
L
H
40
30
20
10
0
r_n, r_{Ti} (cm)
IPP3- BEC 194- 84

Fig. 7